

Experimental and numerical studies on concrete encased embossments of steel strips under shear action for composite slabs with profiled steel decking

Noémi Seres^{1*}, László Dunai^{1a}

¹*Department of Structural Engineering, Budapest University of Technology and Economics,
Műegyetem rkp.3-5, H-1111 Budapest, Hungary*

(Received June 4, 2010, Accepted November 30, 2010)

Abstract. The subject of the ongoing research work is to analyze the composite action of the structural elements of composite slabs with profiled steel decking by experimental and numerical studies. The mechanical and frictional interlocks result in a complex behaviour and failure under horizontal shear action. This is why the design characteristics can be determined only by standardized experiments. The aim of the current research is to develop a computational method which can predict the behaviour of embossed mechanical bond under shear actions, in order to derive the design characteristics of composite slabs with profiled steel decking. In the first phase of the research a novel experimental analysis is completed on an individual concrete encased embossment of steel strip under shear action. The experimental behaviour modes and failure mechanisms are determined. In parallel with the tests a finite element model is developed to follow the ultimate behaviour of this type of embossment, assuming that the phenomenon is governed by the failure of the steel part. The model is verified and applied to analyse the effect of embossment's parameters on the behaviour. In the extended investigation different friction coefficients, plate thicknesses, heights and the size effects are studied. On the basis of the results the tendencies of the ultimate behaviour and resistance by the studied embossment's characteristics are concluded.

Keywords: composite slab; embossment; shear action; pull-out test; numerical modelling; finite element simulation.

1. Introduction

Composite floor is widely used in the building industry in the last decades. The casting of concrete is carried out on corrugated steel plate (as permanent formwork) which is supported by floor beams. The efficiency of the composite slabs depends on the composite action between the steel and concrete structural members. The interlock on the contact surface is firstly based on an adhesive rigid bond which is generated by the set of cement on the steel surface. This interlock is lost as soon as interface slip occurs. Then the longitudinal shear is transferred by friction and/or mechanical bonds. A typically applied mechanical bond is the rolled embossment on the steel surface. Both friction and mechanical bond result in complicated interacting phenomena what can hardly be handled by the classical design methods of shear connectors. This is why the design of composite floors requires completing

* Corresponding author, Ph. D. Student, E-mail: nseres@vbt.bme.hu

experimental tests to determine the shear transferring mechanism and the standardized longitudinal shear force resistance (EN 1994-1-1 2004). Two design methods for the verification of composite slabs are given in standards: the m-k method and the partial shear connection method. The basis of the m-k method was developed by Porter and Ekberg (1968, 1978) by performance test of four point bended one-way composite slab elements. Porter and Ekberg were the first researchers to carry out push tests on profiled sheeting, too. Recently researchers carried out mostly experimental investigations on full-scale slab specimens (Marimuthu et al. 2007) and different type of push-out/pull-out tests on small-scale specimens (Mäkeläinen and Sun 1999, Burnet and Oehlers 2001) to determine the shear bond characteristics for composite slabs. A new simplified method was meantime developed for the design of composite slabs by Crisinel and Marimon (2004) which provides the design of composite floors by its critical section. To describe the steel-concrete connection the authors used small-scale test information.

Theoretical methods were also proposed to calculate the deflections and longitudinal shear behaviour of composite slabs by Marčiukaitis et al. (2006) and Vainiūnas et al. (2006), those calculations, however, were limited to one specified type of profiled steel sheeting.

Numerical models were developed using different finite element software packages to follow the behaviour of composite floor slabs (Veljković 1997, Eldib et al. 2009, Guo and Bailey 2009, Tsalkidikis and Avelas 2010). The layout of the models was in every case the following: the concrete was modelled by solid elements, the steel part was modelled by shell elements and the interlock was modelled by different interface elements; whereof the characteristic of the interface was obtained from performance tests. Despite they give good prediction, the above presented methodologies suffer from a drawback, namely they need essential experimental background.

In the field of numerical simulation an overall parametric study was accomplished by Ferrer et al. (2006) by 3D FEM model application to determine the influence of geometric and physical parameters for rolled embossments, and steel sheeting optimization is carried out based on the proposed model. Despite the promising achievements, the results are not implemented in design method.

The purpose of the current research is to develop a computational method which can predict the behaviour of embossed mechanical bond in order to derive the design characteristics. The paper presents the first part of the research, in which the local behaviour of an individual embossment is investigated by experimental and numerical studies. A pull-out test specimen is designed for the analysis of an individual embossment. In parallel a numerical model is developed to follow the governing ultimate behaviour mode. The model is verified by experimental results. The effect of the geometrical and physical characteristics on the ultimate behaviour are analysed by the proposed model.

2. Experimental program

2.1 Design of the specimens and the measurement technology

The test specimens are designed on the basis of traditional pull-out tests, with the difference that the steel plate is not a half wave of an open through profile (Mäkeläinen and Sun 1999, Burnet and Oehlers 2001), but it has one enlarged embossment, as shown in Fig. 1. The scope of the enlargement of the embossment is to be able to create the specimen and to follow the failure phenomenon by strain gauge measurement. The enlarged embossment is pressed by a 45 mm diameter bearing ball. The bearing ball is pressed 10 mm deep in the thin plate, so that its final height becomes 10 mm, and its diameter becomes 37.4 mm. In this way an about four times bigger connection is formed then a real one (Burnet

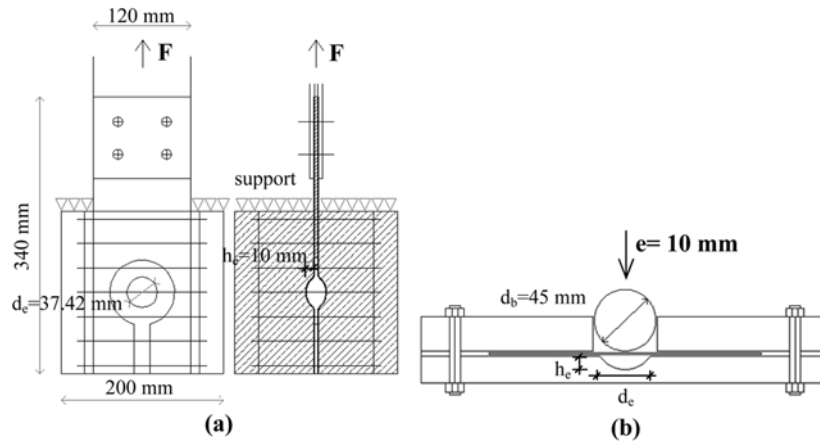


Fig. 1 Test specimens (a) and the extruding process of the embossment (b)

and Oehlers 2001). In order to keep the quasi-original geometric ratio of the embossment, the steel plate thickness is chosen to be thicker than the plate thickness in a regular composite floor; 1.5 and 2 mm. Two thin plates-equipped with the embossment-are placed back-to-back in the middle of a concrete cube. A 6 mm thick spacer plate is installed between the embossed plates. An 80 mm diameter hole is cut on the spacer plate around the embossment, which leave the area of the connection without restraint inside and insures the free deformation of the embossment. The thin plates and the spacer plate are connected on their edges with spot welding, and finally the edges of the plate pile are covered with waterproof adhesive tape, as shown in Fig. 3 (a).

In the design of the specimen it was aimed to avoid the global failure of the concrete block splitting, hence frequently distributed stirrups (by 30 mm) are applied in the concrete block along the plate.

The strains are measured with strain gauges of 1.5 mm of base length. The length/depth dimensions of the grid carrier are 5 and 2.5 mm, respectively.

The strain gauges are placed in two arrangements, as shown in Fig. 2. The strain gauges are glued on the inner face of the embossment. No strain gauges are put on the outer face, since the safe placement of the strain gauges can not be ensured because of the posterior concrete casting. Five base gauges are put on all of the embossed plate pairs and on two of them ten supplementary gauges are also installed. In this way four specimens are made using 5 gauges and two specimens are made using 15 gauges. The positions of the 5 base gauges are determined by the preliminary numerical analysis of the local model (Section 2.2) and these are placed in the axis of symmetry of the embossment according to the

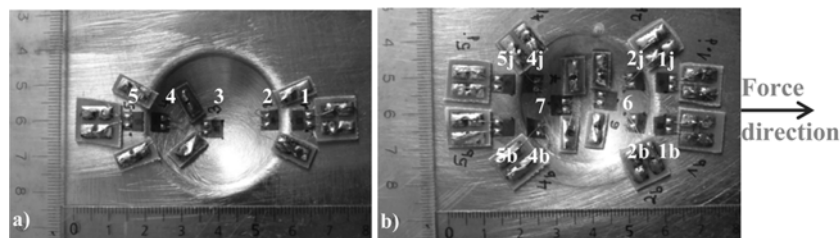


Fig. 2 Strain gauges (a) basic and (b) supplementary

orientation of the load. Gauges #1 and 5 are placed on the plane surface at the bottom edge of the embossment. Gauges #2 and 4 are placed on the opposite side of gauges #1 and 5, respectively on the curved surface. Gauge #3 is put in the middle of the embossment. The role of the other 10 supplementary gauges is to determine the behaviour in the surrounding area of the base gauges. Hence, the gauges are placed next to the gauges #1, 2, 4 and 5 on the right and left side, and also between the gauges #2-3 and 3-4 to be able to follow the entire longitudinal deformation of the embossment. The distance between the strain gauges is shown in Fig. 2. After fixing the strain gauges on the steel surface, they are covered with a thin wax layer, to avoid the water penetration to the strain gauges due to the concrete casting. Altogether six specimens are made, with the details summarized in Table 1.

Besides the strains, the relative displacement between the steel plate and the concrete cube is also measured with inductive transducers. The results of the strain measurement as well as the load and the displacement results are used for the verification of the numerical model. The importance of the strain measurement is to provide additional information on the ultimate behaviour and failure mechanism, since it cannot be followed inside the concrete block; only the undamaged and the completely destroyed states are visible.

2.2 Preparation of the specimens, test execution

The test specimens are made in the cooperation of the Structural Laboratory of the Department of Structural

Table 1 Test specimens

Specimen code	Sheeting thickness [mm]	Strain gauges [pc]	Concrete cube size [cm]	Steel plate size [mm]	Embossment diameter/height [mm]	f_y/f_u^* of steel [N/mm ²]	f_{ck}^{**} of concrete [N/mm ²]
1.1	1,5 mm	5	20 × 20 × 20	340 × 120	37,4/10	444/510	43,35
1.2	1,5 mm	5	20 × 20 × 20	340 × 120	37,4/10	444/510	43,35
1.3	1,5 mm	15	20 × 20 × 20	340 × 120	37,4/10	444/510	43,35
2.1	2 mm	5	20 × 20 × 20	340 × 120	37,4/10	459/534	43,35
2.2	2 mm	5	20 × 20 × 20	340 × 120	37,4/10	459/534	43,35
2.3	2 mm	15	20 × 20 × 20	340 × 120	37,4/10	459/534	43,35

* yield stress/ultimate stress

** compressive strength

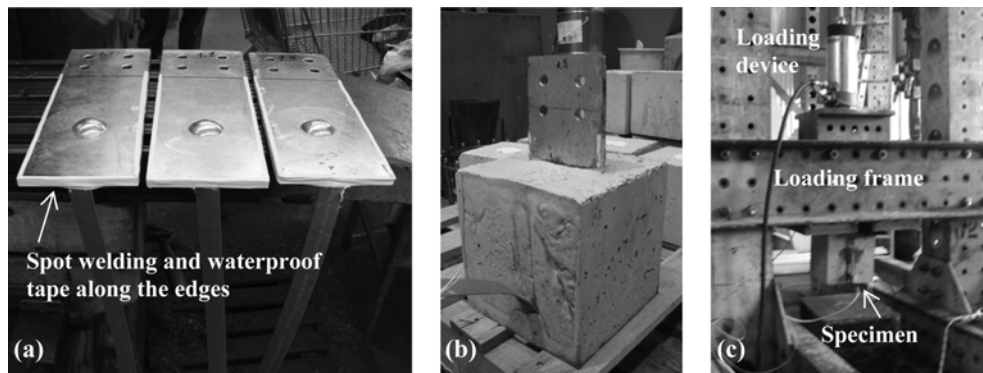


Fig. 3 Specimen preparation (a) plate pairs (b) completed specimen (c) test setup

Engineering and the Laboratory of the Department of Structural Materials and Engineering Geology.

The pull-out test is executed in a loading frame, where the specimen is hung by loading plates which are fixed on the steel overhang of the specimen. The upper surface of the concrete cube is supported from above, as shown in Fig. 1(a) and Fig. 3(c). The load is applied through the loading plates. To insure the centralized and uniform load transfer, and also to correct the concrete surface's irregularity, ~5 mm thick hard rubber pads are used between the loading frame and the concrete cubes' supported surface.

2.3 Material tests

The material properties are determined by additional tests. The measured concrete compressive strength is 43.33 N/mm²; the steel yield strength/ultimate strength are 444/510 N/mm² and 459/534 N/mm² for 1.5 mm and 2 mm thick plate, respectively (Table 1). The full σ - ε curves of the steel materials are also determined from the coupon tests.

2.4 Experimental behaviour of an embossment

As the load is introduced, the first mark of the failure is appeared on the concrete block. The first crack is appeared in line with the steel plate at the exterior surface of the concrete block. The first crack is shown at the side, where the steel plate is closer to. The crack is propagated all over the height of the cube and the steel plate is slipped out from the concrete block. The failed specimen is removed from the loading frame, and the crack pattern on the supported side is analyzed. Two kinds of crack can be identified from the full crack pattern. The first one is parallel with the steel plate and propagates from top to bottom in the concrete cube, and arises also on the supported and the side surfaces. The second one is representative on the supported surface and its near area, and the crack propagates from the edge of the steel plate to the corner of the concrete cube.

Fig. 4 shows two typical measured load-displacement curves. The response of the specimen is almost rigid for the initial loading (2-3 kN). After the behaviour changes and a short linear phase is followed by a nonlinear part, with gradually decreasing slope. From the experimental observation, the end of the linear phase can be identified by a micro crack propagation, which leads to the appearance of the first crack on the concrete surface. After the steel plate slips, a small amount of load increase can be observed till failure. The identification of the characteristic points of the curve is summarized in Table 2.

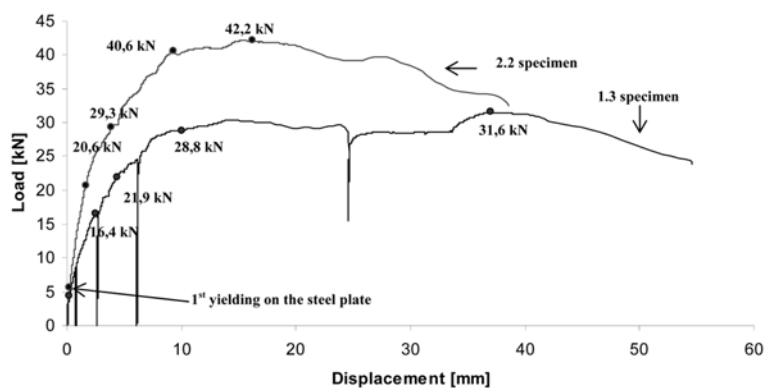


Fig. 4 Load-displacement curves of 1.3 and 2.2 specimens

Table 2 Test results

Sign	End of linear phase [kN]	1 st crack [kN]	Slip of plate [kN]	Ultimate load [kN]	1 st yielding in steel plate [kN]
1.3	16.4	21.9	28.8	31.6	4.39
2.2	20.6	29.3	40.6	42.2	5.62

A significant decrease in the slope can be seen in the curves after the slip of the plate (it indicates the start of the failure mechanism) at an almost the same displacement level of 8-9 mm on every specimen. The global failure, however, occurs after 30-40 mm slips, which shows significant deformation capacity.

In Fig. 5 the observed typical crack pattern and the failure mechanism of the embossment can be seen.

The point of the first yielding on the steel plate, which is marked on both of the curves in Fig. 4, belongs to the strain measurement, when the yielding strain appears at one of the measured points. The value of yielding strain is determined from the material tests. By the evaluation of the measured strains it is found, that the first yielding in the steel plate appears at very low load level (5-10 kN, as shown in Fig. 4) at the bottom of the embossment on the loaded side (at gauge #2 position, Fig. 2). The order of the appearance of yielding at the base gauge positions can be followed in Fig. 6. The values of the load levels referring to yielding are the average of the three specimens of the same kind.

From the experimental observations it can be concluded that the concrete cracking effects the first phase of the behaviour; the ultimate behaviour is governed by the failure of the steel embossment.

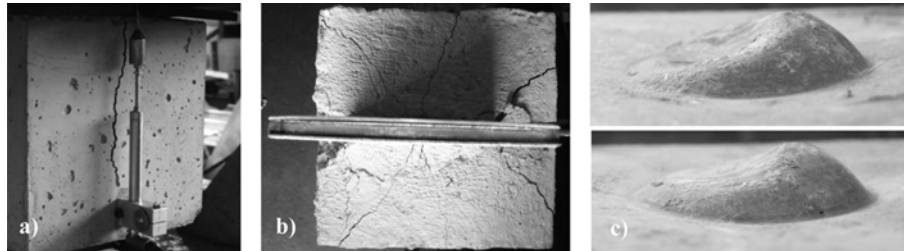


Fig. 5 Crack patterns (a, b) and failure mechanism (c)

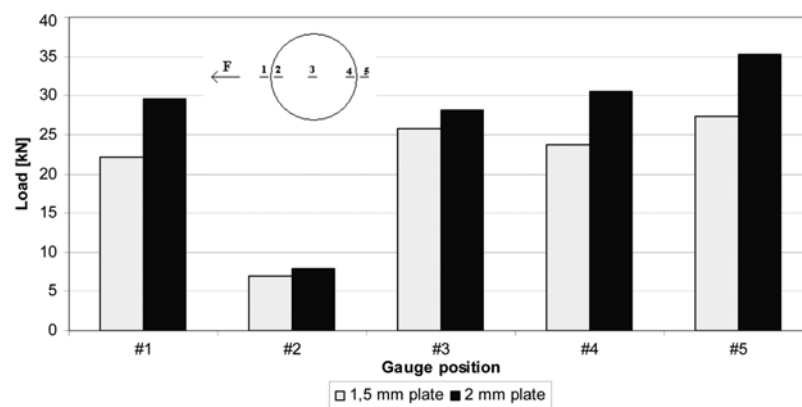


Fig. 6 Yielding at gauge positions

3. Numerical modelling and analysis

3.1 Local model for an individual embossment

3.1.1 Modelling aspects

The purpose of the local model is to analyze the behaviour and the failure mode of an individual embossed mechanical bond.

As it can be seen from the tests the behaviour of the steel and concrete interaction is a highly nonlinear problem. The steel besides the material nonlinear behaviour sustains large strain/displacement during failure. The concrete cracks in tension and crushes in compression in the relevant regions around the embossment. The interlock between the two materials is characterized by contact and friction phenomena of the surfaces. The behaviour of the embossments can be followed by a complex finite element model, where (i) the steel part is modelled by shell elements, (ii) the surrounding concrete block is modelled by solid elements, and (iii) the interlock between them is represented by a sliding contact with friction, which is defined on the shell and solid contact surfaces. Based on this concept a fictive local model was worked out by the authors (Seres et al. 2008). The local model composed of a section of steel sheeting with one embossment on its surface, and the surrounding concrete block. The load was applied as surface load on the face of the concrete block and the purpose of the analysis was to push-out the concrete block from the steel sheeting, and to derive the failure characteristics. During the modelling and testing process it was found that the complexity of the model resulted in significant computational difficulties, which arose the question of the model applicability.

A simplification of the model can be made, if the steel plate in the structure is relatively weaker comparing to the concrete (as in the case of the completed experiments), which means that the steel behaviour dominates in the global failure. Having this assumption the concrete block is assumed to be rigid and non-damageable part in the model. The proposed solution for that case is to replace the concrete solid elements with a rigid shell surface in the finite element model: the steel part is modelled with shell elements, and the solid part is ignored, and a rigid shell surface with identical geometry like the embossment is considered instead. The interlock characteristics between the two surfaces remain the same as in the complex model. In the analysis the surface with steel properties is pulled out from the rigid one, considering the contact and friction between them.

3.1.2 Finite element model

On the basis of the above idea a numerical model is developed in ANSYS finite element program (ANSYS® v11.0). The SHELL181, 4-node finite strain shell element is applied in the model, which is suitable for analyzing thin and moderately thick shell structures. A 5 mm maximum element size is applied in the finite element mesh. The effect of the mesh density is analyzed, as detailed in Section 3.2. As interface element, a surface-to-surface contact pair is employed: the Conta173 is used to represent contact and sliding between 3D target surfaces (Target 70) and a deformable surface, defined by this element. These elements are applicable to 3D structural and coupled field contact analyses. It has the same geometric characteristics as the solid or shell element face with which it is connected. Contact occurs when the element surface penetrates one of the target segment elements on a specified surface. Isotropic Coulomb friction is applied in the model which is specified by a single coefficient of friction.

A quarter of the full specimen is modelled, and it is composed of two surfaces: (i) the embossed shell surface with steel material properties and (ii) the finite element mesh of target surface, which represents the rigid concrete block. The target surface is rigid by restraining all of its DOF's. The contact finite

element mesh is defined on the steel part of the interface. The embossed plate is composed of two parts: (i) the area of the embossment and (ii) the area of the spacer plate. The area of the embossment is left without restraint, while the transversal displacement is avoided along the spacer plate's surface. The load is applied on the model by prescribed displacements at the end of the steel plate. The details and the layout of the model are summarized in Table 3 and in Fig. 7.

A multi-linear (linear elastic-hardening plastic) material model is applied for the steel plate (elastic modulus $E = 213.5$ GPa, Poisson's ratio $\nu = 0.3$). The characteristics of the material model are based on the material test results, and it is determined by four characteristic points: (1) yield stress, (2) starting of hardening, (3) ultimate stress, (4) ultimate strain. The material model is determined for both 1.5 mm and 2 mm thick plate; the characteristics can be found in Table 4, and Fig. 8. The material of steel is considered as homogenous, isotropic and described with the multi-linear model detailed above, all over the steel surface.

3.1.3 Nonlinear solution technique

The Newton-Raphson approach is used in the nonlinear analysis. The convergence of the solution is checked on the basis of the Euclidean norm of unbalanced force vector by applying a tolerance of 0.1%. In the geometric nonlinear analysis large displacements and strains are considered. Automatic time stepping is used which cut a time step size in half whenever equilibrium iterations fail to converge and

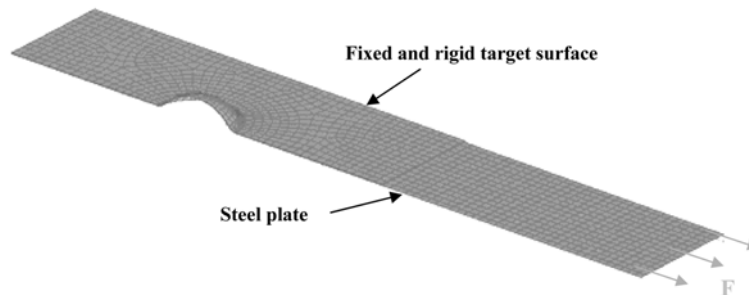
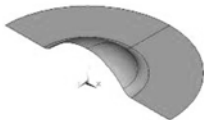
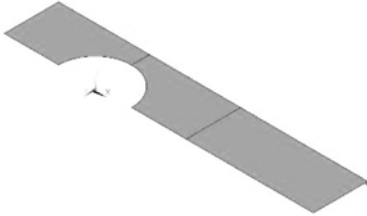
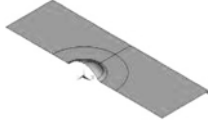


Fig. 7 The FE model

Table 3 Details of the FE model

Model part	Steel			Concrete
	Embossment area	Spacer plate		Interface area
Figure				
Position	Under target	Under target	Overhang	Target
Finite element	SHELL181+CONTA173	SHELL181+CONTA173	SHELL181	TARGE170
Mat. model	Multi-linear	Multi-linear		Friction
DOF	No constraint	Transversal fixed		All fixed

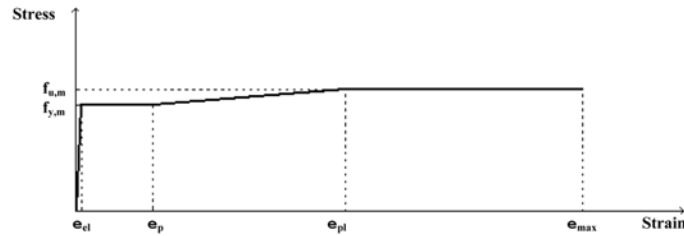


Fig. 8 Material model for steel

Table 4 Characteristic points of the material model

Plate thickness	1,5 mm		2 mm	
Curve points	Stress [N/mm ²]	Strain [%]	Stress [N/mm ²]	Strain [%]
(1) yield stress	444	0.208	459	0.23
(2) start of hardening	444	3.204	459	2.88
(3) ultimate stress	510	11.285	534	8.79
(4) ultimate strain	510	21.17	534	18.83

automatically restart from the last converged sub step. If the halved time step again fails to converge, bisection will again cut the time step size and restart, continuing the process until convergence is achieved or until the minimum time step size is reached.

3.2 Mesh sensitivity analysis

In the first step, the model is meshed with uniform finite elements with 5 mm edges. The obtained load - displacement curve can be seen in Fig. 9. The curve shows waving character, what is caused by the abrupt change of the contact. To check the effect of discretisation, a mesh sensitivity analysis is carried out with refining the mesh around the area of the embossment.

Four mesh sizes are studied by a maximum element edge length of 5 mm to 2 mm. The results in Fig. 9 show that the global characters of the curves remain the same; the ultimate loads are practically the same, but the curves become smoother by decreasing the mesh size. Based on the results it is concluded

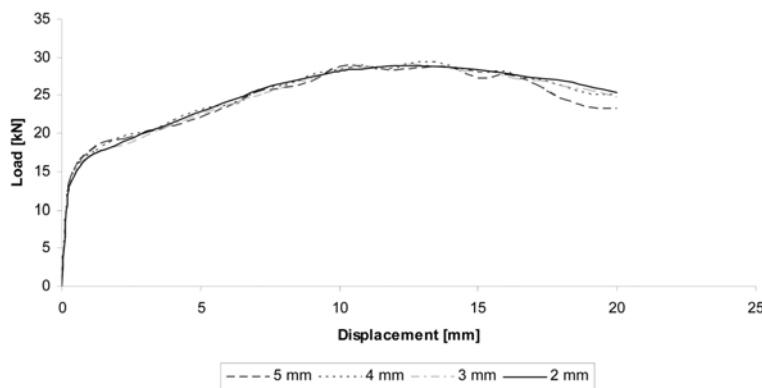


Fig. 9 Results of mesh sensitivity analysis

that the behaviour of the interface elements is influenced by the mesh size, which locally disturbs the characteristics of the load - displacement curve.

3.3 Analyses and results

3.3.1 Numerical and experimental behaviour

Nonlinear analysis is completed on test model by applying kinematic load, with 20 mm maximum displacement. This displacement is identified as the start of the development of failure mechanism in the tests. The results show good agreement with the experiments, as it can be seen in the load - displacement curves in Fig. 10.

The initial quasi-linear phase is longer in the numerical result, and its slope is higher, compared to the experimental curve. The yielding plateau type behaviour is obtained thereafter. Two effects which play role in the experiment are not considered in the model: (a) the effect of the extruding process of the embossment is not taken into account in the material model and (b) the concrete is simplified in the model and its damages are not considered. Based on experimental observation, the decreasing of the slope of the experimental curve overlap with the appearance of the cracking on the concrete surface as detailed in Section 2.4. Serious delamination between the concrete and the steel plate is not observed, since the crack opening is relatively small around the plate due to the stirrups, which hold the concrete block in a whole. Since, the applied model does not contain concrete; this local phenomenon cannot be followed. No information is possessed about the possible effect of the cold forming of the connection. Thus the reason of the initial deviation between the experimental and the numerical curve is difficult to unambiguously judge. It can be the combined effect of the internal concrete damages and the cold forming.

Good agreement can be seen, however, between the experimental and the numerical curves in the range of ultimate behaviour. In this phase the source of the nonlinearity is the steel yielding of the embossment whereof the applied model gives correct prediction.

3.3.2 Characteristics of the load-displacement relationship

A typical load-displacement curve is presented in Fig. 11, showing its characteristic points. The points indicate the relevant yield pattern, evaluated by von Mises plastic strain distribution, and the embossment's deformation.

A quasi-linear first phase can be observed on the curve till first yielding appears on the loaded side of

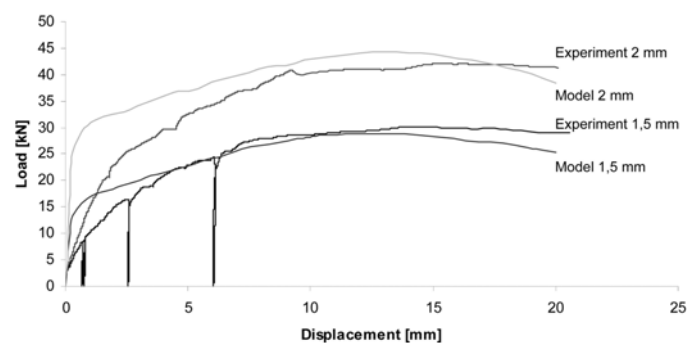


Fig. 10 Experimental vs. numerical results

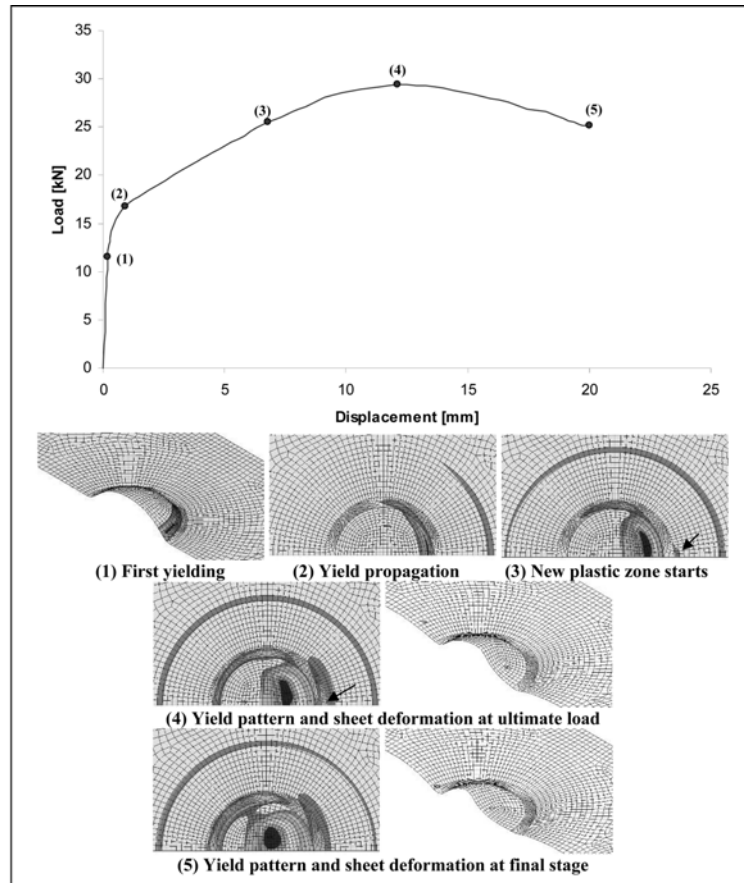


Fig. 11 Observed numerical behaviour

the embossment (1st point). Increasing the load, the yielding zone spreads around the embossment from front to back. As the yielding zone reaches halfway around the embossment (2nd point), it starts to expand from the bottom to the top of the embossment, on the loaded face. This phenomenon is followed by a significant decrease in the slope. The 3rd point on the diagram belongs to the appearance of a new plastic zone, on the plane surface, in front of the embossment's loaded side. The propagation of the yielding zones leads to the failure. The 4th point represents the ultimate load (28.88 kN at a displacement of 11.87 mm). The 5th point shows the load belonging to the ultimate displacement (20 mm).

3.3.3 Strain measurement

The evaluation of the strain results are made in the specified nodes. Typical results of the strain measurement can be seen in Fig. 12. The curves show the relationship of the load and the strain in the centre of the embossment comparing it with experimental results (gauge #3). A good agreement can be seen on the global characteristics of the numerical and experimental results, at the initial phase, a difference can be observed, however, in the slopes.

The difference can explained both by the model and by the measurement. With the extruding process a significant residual strain is introduced in the steel plates around the embossment, what is not considered in the model. Beside this most of the strain gauges are put on curved surface, and the

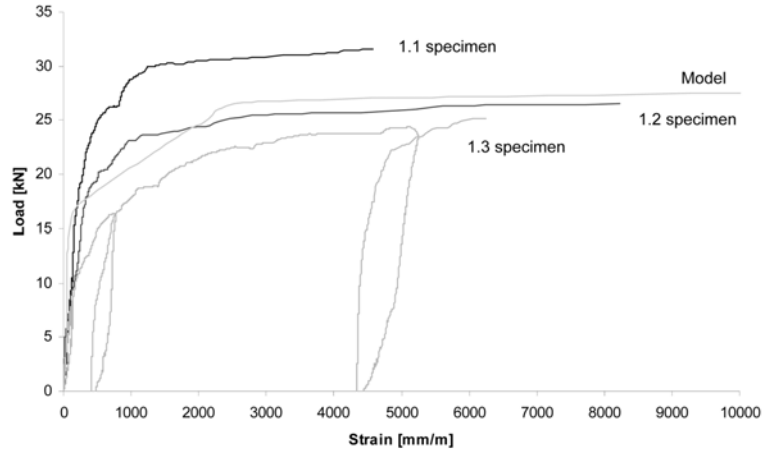


Fig. 12 Strains in the middle of the embossment (gauge #3)

precision of the measured values can be influenced by this fact.

By comparing the strain results of the measurement and the numerical model, it is found that the arrangement of the strain gauges is appropriate to provide results for the verification; and the strain gauges follow well the behaviour of the embossment's failure.

3.3.4 Evaluation of the numerical model

From the results it can be seen that the model can follow accurately the ultimate behaviour if it is governed by the steel plate failure.

Despite the differences in the numerical and experimental behaviour in the first phase of the load-displacement relationship the ultimate load and failure mode are well predicted. The computational efficiency of the model is good; the running time of a typical model with 5 mm/2 mm of maximum element edges having 10 506/27 066 DOF's is 7/31 minutes (Intel P4 3 GHz, 2 GB RAM).

On this basis the model is found to be accurate and efficient enough to study the ultimate behaviour of this type of embossment.

4. Effect of the embossment's parameters on the ultimate behaviour

An extensive parametric investigation is carried out by the developed model to study the ultimate behaviour of an embossment by changing the geometric and physical characteristics: the plate thickness, the coefficient of friction and the height of the embossment in the model.

4.1 Coefficient of friction

The coefficient of friction is a very scattered physical magnitude, what characterises the quality of the contact surfaces (Ferrer et al. 2006). The analysis is carried out on three plate thicknesses, with increasing the value of the coefficient of friction from 0-0.6 in a step of 0.1. All of the values are applied on the 1.5 mm thick plate, and three of them are chosen for the other two plate thicknesses.

It is found that the load carrying capacity increases approximately threefold with increasing the

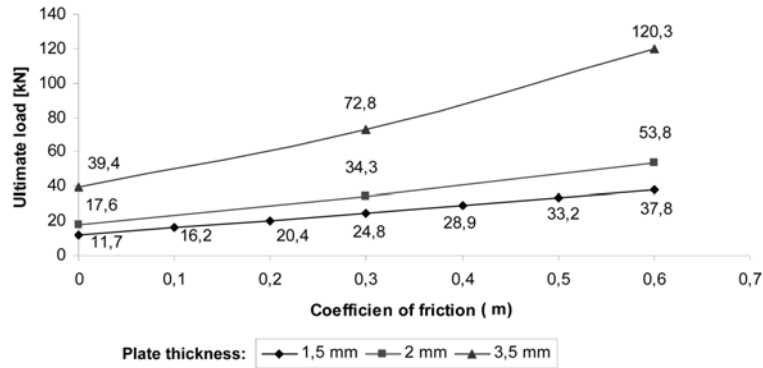


Fig. 13 Effect of the coefficient of friction on the load carrying capacity

coefficient of friction from the minimum to the maximum value, and the tendency is quasi-linear, as shown in Fig. 13.

4.2 Plate thickness

Based on previous experimental investigations (Marimuthu et al. 2007) the sheeting thickness is an important influential factor of the load carrying capacity and also of the initial stiffness. Seven plate thicknesses are applied on the model from 0.5 to 3.5 mm, in a step of 0.5 mm.

The load carrying capacity is more than eightfold higher on the 3.5 mm thick plate compared to the 0.5 mm thick plate. Fig. 14 illustrates, that the relationship between the load carrying capacity and the sheeting thickness can be approximated with a 2nd order function what reflects the dominant bending type failure of the plate.

4.3 Embossment height

The effect of changing the height of the embossment is analyzed by taking the maximum height of the embossment as 10 mm (experimental value) and it is decreased by taking 2.5 mm sections to the 2.5 mm minimum value of the embossment, as shown in Fig. 15. In the experiment, the ratio between the

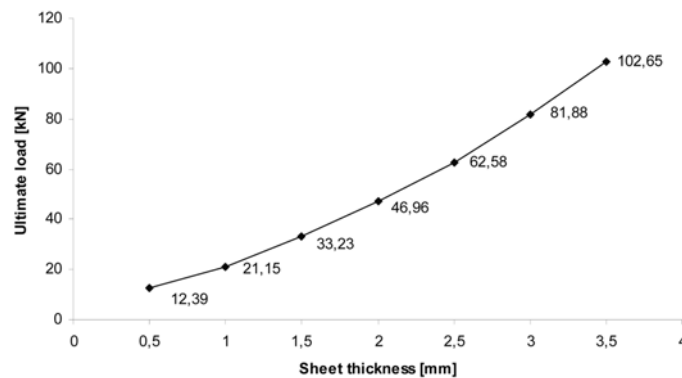


Fig. 14 Effect of the plate thickness on the load carrying capacity

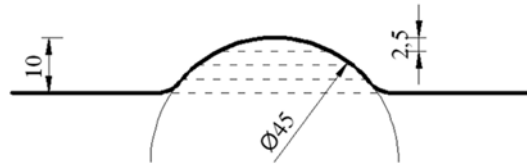


Fig. 15 Section levels

embossment diameter and the diameter of the spacer plate's hole is $80 \text{ mm}/37.4 \text{ mm} = 2.14$. It determines the area of the embossment which is left without restraints compared to the embossment's diameter. The original ratio between the diameters is kept in case of every embossment height.

4.3.1 Effect on the behaviour

The behaviour is determined for 1.5 mm plate thickness. The results are illustrated by the load-displacement curves in Fig. 16, and by the plastic zones in Table 5. The evaluation is based on the characteristic curve points of 10 mm height embossment, as introduced in Section 4.2.1. The tendencies of the behaviour are explained as follows:

Load – displacement relationship

The load-displacement curves of the embossments of 5/7.5/10 mm heights are composed of four parts, namely a (i) linear phase, a (ii) nonlinear part with gradually decreasing slope, a (iii) yielding accompanied with large displacement and a final (iv) descending phase. The load-displacement curve of the embossment of 2.5 mm height on the other hand composes of three phases. The above mentioned third curve part is missing, so the descending phase follows immediately the end of the nonlinear part. It means that the appearance of the additional plastic zone brings also the reach of the ultimate load, as clearly shown in Fig. 16.

Yielding propagation

In every case the end of the linear phase on all of the load displacement curves belongs to the appearance of the first yielding at the bottom of the embossment on the loaded side (as in Fig. 11/detail 1 and also in the 1st column of Table 5.). The end of the nonlinear part belongs to the phenomenon, when the yielding zone reaches halfway around the embossment (as in Fig. 11/detail 2).

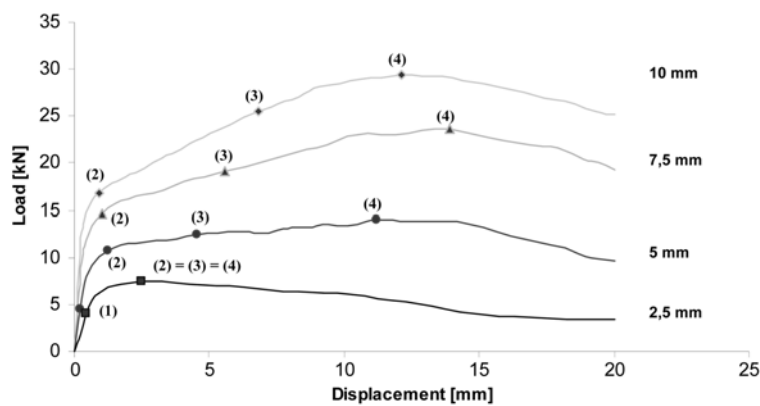
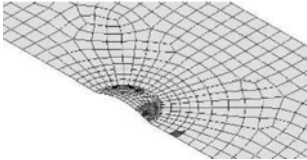
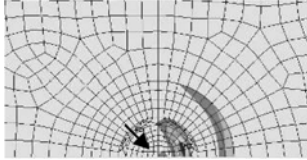
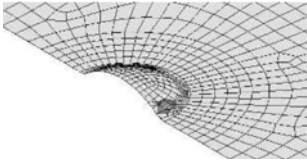
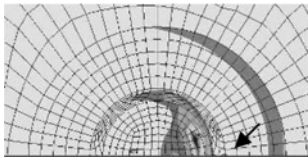
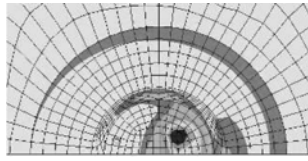
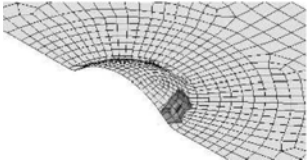
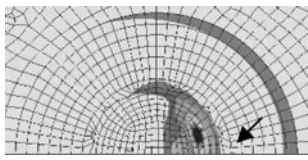
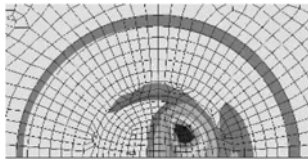
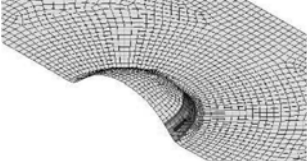
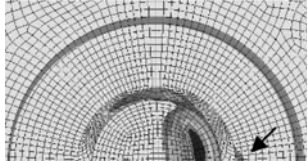
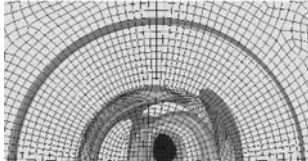


Fig. 16 Effect of the height of the embossment on the behaviour

Table 5 Propagation of plastic zones for different heights of embossment

Height [mm]	End of the linear phase yielding appears (1)	Additional plastic zone (3)	Ultimate load yield pattern (4)
2.5			
5			
7.5			
10			

When the appearance and the propagation of yielding is analysed on the models, it is observed that for the embossments of 5/7.5/10 mm heights an additional plastic zone appears on the plane surface in front of the embossment's loaded side, as it is shown in the second column of Table 5. This additional yielding zone for the embossment of 2.5 mm height appears in the middle of the embossment.

For the embossment of 2.5 mm height the plastic zone propagates practically equally from the loaded side to the back. When increasing the height from 2.5 mm to 10 mm the separation between the plastic zone on the front of the embossment and the plastic zone around the embossment is getting more significant.

The load-displacement relationship in case of 2.5 mm height decreases after the end of the first nonlinear phase, while in the case of the other heights the load is increasing after this point (curve sections between the markers (3) and (4) in Fig. 16). The load increment is accompanied with large deformation of the embossment. The phenomena are well illustrated by the deformed shape at ultimate load level in Fig. 17. In case of 2.5 mm height, the embossment keeps almost its original shape till ultimate load, while the other embossment sustains significant deformations before reaching the ultimate load.

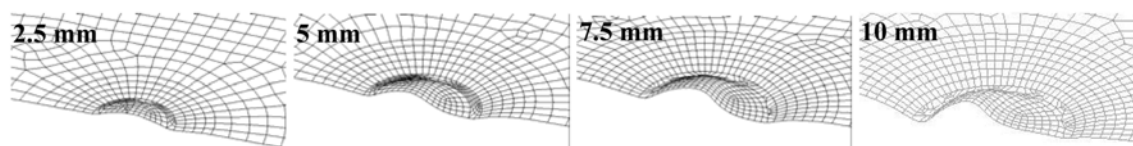


Fig. 17 Deformation at ultimate load for different embossment heights

4.3.2 Effect on the load carrying capacity

The four embossment heights are analyzed by applying three plate thicknesses to determine the tendencies on the load carrying capacity. It is found that the load carrying capacity increases quasi-linearly with increasing the height of the embossment, as it is shown in Fig. 18. The most dominant increment in load carrying capacity is observed in the case of 1.5 mm plate thickness.

4.4 Size effect

4.4.1 The purpose of the study

After the effect of basic parameters is determined, the relationship between the experimental enlarged embossment and a real sized embossment with similar geometric ratios is analysed. The height of the embossment is reduced proportionally with its diameter (to keep the original embossment ratio), from the experimental size to a real embossment size (Burnet and Oehlers 2001). Four embossment sizes are taken from 10 mm to 2.5 mm height, in a step of 2.5 mm, as shown in Fig. 19.

Comparing the results to the height analysis, same heights of embossment are analysed with 1.5 mm plate thickness and a value of coefficient of friction 0.5. Comparing to the height analysis, the surface of the embossment is always smaller and the embossing slope is always higher by the size effect analysis, as shown in Fig. 20. The reference embossment height/size is always the experimental embossment geometry ($h = 10$ mm, $d = 37.4$ mm, $\alpha = 56^\circ$). The size effect analysis in this way involves the slope effect, too.

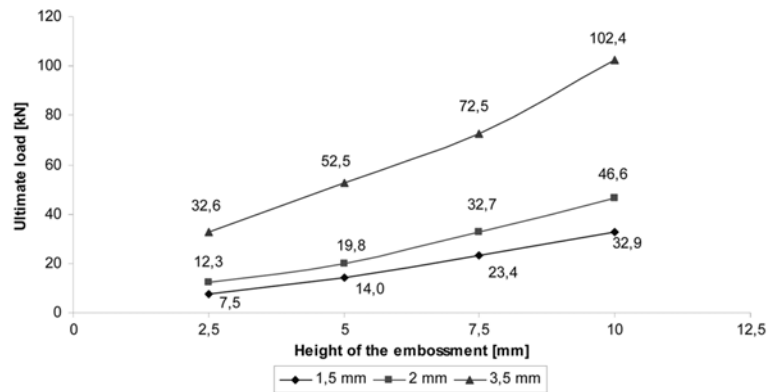


Fig. 18 Effect of the height of the embossment on the load carrying capacity

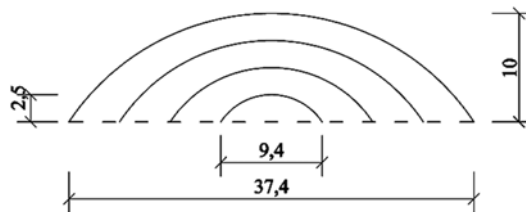


Fig. 19 Embossment size reduction

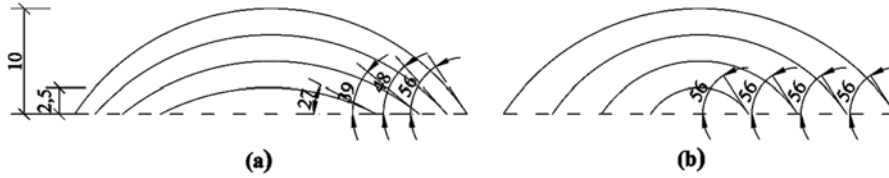


Fig. 20 Embossing slope for (a) height and (b) size effect analysis

4.4.2 Size effect on the behaviour

The effect of the embossment size (considering the embossing slope effect) can be analyzed by the load-displacement curves, shown in Fig. 21. Comparing to the load-displacement relationships of the height analysis the character of the curves remains similar.

The same evaluation method is chosen for the size effect analysis as in the case of height analysis. The end of the linear phase (1) which is identified with the appearance of the first yielding on the steel plate is followed by a nonlinear curve section which belongs to the spreading of the plastic zone in front of the embossment. The end of the nonlinear part (2) in case of 2.5 mm size is identical with the ultimate load, and in case of the other heights the load is increasing after this point while the displacements become large. In case of 5 mm size the end of the linear phase (2) is identical with the appearance of an additional plastic zone (3) on the top of the embossment. In case of 7.5-10 mm heights the additional plastic zone appears on the plane surface in front of the embossment (3). Point (4) represents the ultimate load which appears besides increasing displacements when increasing the size of the embossment.

The propagation of the plastic zones can be followed by the pictures of Table 6. In case of 2.5 mm and 5 mm size the plastic zone concentrates on the front side of the embossment. In case of size 7.5 mm (and also 10 mm) the plastic zone separates on two parts and it is propagating around the bottom of the embossment and on the front side. The deformation at ultimate load can be seen in Fig. 22. It is shown on the pictures that the smallest embossment fails after relatively small deformations while the other sizes fail after large deformations.

4.4.3 Effect on the load carrying capacity

Analysing the four embossment sizes it is found that the load carrying capacity increases quasi-linearly with increasing the size of the embossment, as it is shown in Fig. 23 in the same diagram with the height analysis results. The observed load carrying capacity is always higher for the same height in

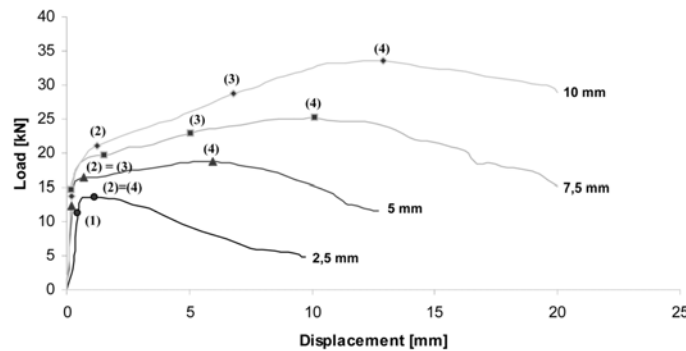


Fig. 21 Size effect on the behaviour

Table 6 Propagation of plastic zones for different size of embossment

Height [mm]	End of the linear phase yielding appears (1)	Additional plastic zone (3)	Ultimate load yield pattern (4)
2.5		-	
5			
7.5			
10			

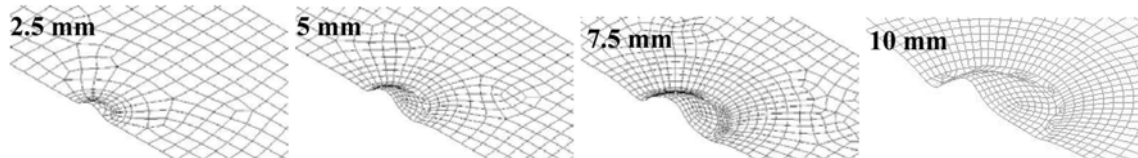


Fig. 22 Deformation at ultimate load for the different embossment sizes

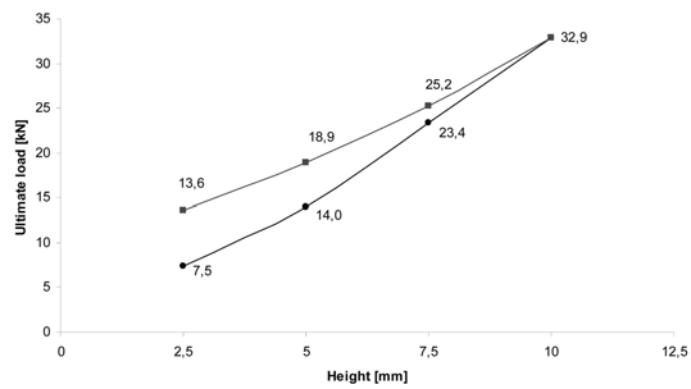


Fig. 23 Size effect on the load carrying capacity

case of size effect results compared to the results of the height analysis. It is found that the highest difference in load carrying capacity occurs where the difference between the embossing slopes is the biggest. Based on prior research (Ferrer et al. 2006) the embossing slope is the most important parameter and the dependency of sliding resistance is significant.

5. Summary and conclusions

In the paper an experimental and numerical investigation of concrete encased embossments of steel strips under shear action is presented.

An enlarged novel test specimen is introduced to study the local behaviour of an individual embossment. The basic behaviour modes of the studied arrangement are observed from the tests and can be summarized as follows:

- the initial phase of the behaviour is influenced by concrete cracking;
- the ultimate behaviour is governed by the failure of the steel embossment (weaker steel embossment comparing to the surrounding concrete).

A finite element model is developed and verified on the basis of experimental results. In the model it is assumed that in the ultimate behaviour the steel part dominates, ignoring the concrete damages. By the comparison of the experimental and numerical results it is found that:

- in the range of the initial behaviour the calculated results show higher stiffness due to the elimination of concrete cracking;
- the results show good agreement in the range of ultimate behaviour;
- the failure mechanism of the embossment and the load carrying capacity can be predicted with good accuracy;
- the computational method is accurate and efficient and it can be applied in further research.

A parametric study is completed by the developed model, to determine the effect of the following embossment's parameters on the ultimate behaviour: coefficient of friction, plate thickness and height; in addition size effect analysis is also completed on embossments with reduced sizes. From the results the following conclusions can be drawn:

- the load carrying capacity is increased linearly as the coefficient of friction and the height of the embossment is bigger;
- different ultimate behaviour and failure mechanisms are obtained by decreasing the height of the embossment;
- the effect of the plate thickness on the load carrying capacity can be characterized by second order relationship;
- the load carrying capacity depends linearly on the embossment size and the same type of ultimate behaviour is obtained as in the case of the height analysis;
- degradation of the deformation capacity is observed by reducing the size of the embossment.

Further research is planned on the following directions: (i) numerical model development for the analysis of different embossment geometries, (ii) experimental and numerical investigations applying a series of spherical embossments, (iii) involving concrete damage in the analysis and (iv) study the effect of the cold forming on the behaviour.

Acknowledgments

The presented research is conducted under the financial support of the OTKA T049305 project, Hungary.

References

- Burnet, M.J. and Oehlers, D.J. (2001), "Rib shear connectors in composite profiled slabs", *J. Constr. Steel Res.*, **57**(12), 1267-1287.
- Crisinel, M. and Mariomon, F. (2004), "A new simplified method for the design of composite slabs", *J. Constr. Steel Res.*, **60**(3-5), 481-491.
- Eldib, M.E. A-H, Maaly, H.M., Beshay, A.W. and Tolba, M.T. (2009), "Modelling and analysis of two-way composite slabs", *J. Constr. Steel Research*, **65**(5), 1236-1248.
- Ferrer, M., Marimon, F and Crisinel, M. (2006), "Designing cold-formed steel sheets for composite slabs: An experimentally validated FEM approach to slip failure mechanics", *Thin. Walled. Struct.*, **44**(12), 1261-1271.
- Marčiukaitis, G., Jonaitis, B. and Valivonis, J. (2006), "Analysis of deflections of composite slabs with profiled sheeting up to the ultimate moment", *J. Constr. Steel Res.*, **62**(8), 820-830
- Marimuthu, V., Seetharaman, S., Jayachandran, A.A., Chellappan, A., Banndyopadhyay, T.K. and Dutta, D. (2007), "Experimental studies on composite deck slabs to determine the shear-bond characteristic (m-k) values of the embossed profiled sheet", *J. Constr. Steel Res.*, **63**(6), 791-803.
- Mäkeläinen, P. and Sun, Y. (1999), "The longitudinal shear behaviour of a new steel sheeting profile for composite floor slabs", *J. Constr. Steel Res.*, **49**(2), 117-128.
- Tsalkatidis, T. and Avdelas, A. (2010), "The unilateral contact problem in composite slabs: Experimental study and numerical treatment", *J. Constr. Steel Res.*, **66**(3), 480-486.
- Vainiūnas, P., Valivonis, J., Marčiukaitis, G. and Jonaitis B. (2006), "Analysis of longitudinal shear behaviour for composite steel and concrete slabs", *J. Constr. Steel Res.*, **62**(12), 1264-1269.
- Veljković, M. (1998), "Influence of load arrangement on composite slab behaviour and recommendations for design", *J. Constr. Steel Res.*, **45**(2), 149-178.
- Seres, N., Joó, A.L. and Dunai, L. (2008), "Numerical modelling of shear connections for composite slabs", *Proceedings of the Ninth International Conference on Computational Structures Technology*, Civil-Comp Press, Stirlingshire UK, Paper 303, doi:10.4203/ccp.88.303.
- Guo, S. and Bailey, C. (2009), "Experimental and numerical research on multi-span composite slab", *Proceedings of the 9th International Conference on Steel Concrete Composite and Hybrid Structures*, Research Publishing Services, ISBN 978-981-08-3068-7.
- ANSYS® v11.0, Canonsburg, Pennsylvania, USA.
- EN 1994-1-1 (2004), Eurocode 4: *Design of composite steel and concrete structures-Part 1.1 General rules and rules for buildings*.
- Porter, M.L. (1968), "Investigation of light gauge steel forms as reinforcement for concrete slabs", *MS Thesis*, Iowa State University, Ames, Iowa.
- Porter, M.L. and Ekberg, C. (1978), "Compendium of ISU research conducted on cold-formed steel-deck-reinforced slab systems", *Eng. Res. Ins.*, Iowa State University, Ames, Iowa.